



General numerical implementation of a new piezoelectric shunt tuning method based on the effective electromechanical coupling coefficient

Toftekær, Johan Frederik; Benjeddou, Ayech; Høgsberg, Jan

Published in:
Mechanics of Advanced Materials and Structures

Link to article, DOI:
[10.1080/15376494.2018.1549297](https://doi.org/10.1080/15376494.2018.1549297)

Publication date:
2020

Document Version
Peer reviewed version

[Link back to DTU Orbit](#)

Citation (APA):
Toftekær, J. F., Benjeddou, A., & Høgsberg, J. (2020). General numerical implementation of a new piezoelectric shunt tuning method based on the effective electromechanical coupling coefficient. *Mechanics of Advanced Materials and Structures*, 27(22), 1908-1922. <https://doi.org/10.1080/15376494.2018.1549297>

General rights

Copyright and moral rights for the publications made accessible in the public portal are retained by the authors and/or other copyright owners and it is a condition of accessing publications that users recognise and abide by the legal requirements associated with these rights.

- Users may download and print one copy of any publication from the public portal for the purpose of private study or research.
- You may not further distribute the material or use it for any profit-making activity or commercial gain
- You may freely distribute the URL identifying the publication in the public portal

If you believe that this document breaches copyright please contact us providing details, and we will remove access to the work immediately and investigate your claim.

General numerical implementation of a new piezoelectric shunt tuning method based on the effective electromechanical coupling coefficient

Johan Frederik Toftekær¹, Ayeche Benjeddou^{2,3} and Jan Høgsberg¹

¹Department of Mechanical Engineering, Technical University of Denmark, Kgs. Lyngby, Denmark
e-mail: jotof@mek.dtu.dk, jhg@mek.dtu.dk

² Université de Technologie de Compiègne, CNRS, ROBERVA, Compiègne, France
e-mail: ayeche.benjeddou@utc.fr

³SUPMECA, 3 Rue Fernand Hainaut, 93407 Saint Ouen, France
e-mail: benjeddou@supmeca.fr

Abstract

A recently proposed tuning method for resistive-inductive (RL) shunts is implemented in a commercial finite element (FE) code (ANSYS®). A main result of the paper is therefore the consistent formulation of the tuning method in terms of variables directly available as solutions in any commercial FE code: The two natural frequencies associated with short- and open-circuit (SC and OC) electrodes and a modal charge obtained as the electrical SC reaction force. An alternative method is based on quasi-static solutions with SC and OC electrodes, convenient for both numerical analysis and experiments. The proposed shunt tuning method is suitable for implementation in any commercial FE software supporting electromechanical analysis and ANSYS® has been used to assess its accuracy for a piezoelectric smart plate benchmark problem. The method is finally extended to multiple piezoceramic patches, placed symmetrically on the structure and shunted to a single RL network, whereby more vibration modes can be effectively controlled for the specific plate problem.

1 Introduction

Piezoelectric transducers attached locally to a host structure enable dissipation of converted mechanical energy into heat by a supplemental resonant shunt. The latter is often designed as a series or parallel connection of a resistance (R) and an inductance (L), whereby the effect on the host structure from the electromechanical transducer corresponds to an inerter-based absorber [1]. The RL -shunt circuit was first suggested and experimentally demonstrated by Forward [2]. Actual calibration procedures were subsequently derived first for the series [3] and since for the parallel shunt circuit [4]. Both calibration methods are based on a single mode representation of the vibrating host structure and are governed by the resonant frequency of a targeted vibration form and the capacitive properties of the piezoelectric transducer(s).

Recently, the modal coupling introduced by the presence of a supplemental absorber on the structure has been represented in [5] via the dynamic characteristics of the other non-resonant modes around the targeted resonant frequency. It demonstrated the ability of two consistent correction terms to accurately account for both the flexibility and inertia effects from residual modes and to adjust the absorber tuning to retain a desired flat plateau in the frequency response curves. The initial analysis for mechanical tuned mass- and inerter-based absorbers [5] has recently been extended to RL -shunted piezoelectric transducers [1].

The performance of a piezoelectric transducer is inherently limited by its capacitive property, which is inversely proportional to the stiffness of an equivalent mechanical absorber. A key factor in the electromechanical absorber tuning has therefore been the accurate representation and maximization of the effective (or generalized) electromechanical coupling coefficient (EMCC). The latter represents the apparent electromechanical to modal stiffness ratio and thus the relation between the inherent capacitance, electromechanical coupling and structural resonance. In [6], a piezoelectric shunt tuning procedure has been derived on the basis of the effective

EMCC, demonstrating its direct equivalence to a modal EMCC with residual corrections from non-resonant modes. The effective EMCC is therefore a key parameter for electromechanical structures; it is commonly defined by the relative difference between (the square of) the associated short circuit (SC) and open circuit (OC) frequencies [7]. Consequently, it is a measure for the level of attainable damping and has therefore been the objective for the design and optimization of piezoelectric transducer systems [8]. It is possible to increase the effective EMCC - and thereby the attainable damping - by the application of a negative capacitance in the electric shunt circuit [9]. Unfortunately, this increases the required shunt inductance, which is usually so large that it must already be realized by active electronic shunt components. Thus, the absorber realization is often limited by the magnitude of the shunt inductance instead of the inherent transducer capacitance. However, it has recently been demonstrated that even large inductances can be obtained by simply winding a copper wire around a magnetic core [10], which substantially improves the feasibility of genuine passive shunts [11]. The present work concerns pure passive vibration control, in which case the attainable damping is governed by the magnitude of the transducer capacitance with the magnitude of the EMCC as a limiting factor in the design of the transducer and the corresponding shunt tuning procedure.

In the present work, a recently proposed shunt tuning method, based on the effective EMCC, is implemented in the commercial finite element (FE) code ANSYS® [12]. Correction terms, that represent the interaction with non-resonant modes, are consistently derived from the natural frequencies obtained by the three eigenvalue problems associated with piezoelectric SC and OC electrodes and a pure inductive shunt. However, as demonstrated in [13], the solution for the pure inductive shunt is only needed when the effective EMCC is almost vanishing because of a very indirect location of the transducer(s). Therefore, in most practical problems, the tuning formulae only rely on the two natural frequencies from the SC and OC limits and a modal charge that appears as a supplemental reaction force associated with SC electrodes. This tuning procedure is simply and very directly implemented in a commercial FE code. The present tuning method is implemented in ANSYS®, which supports three-dimensional (3D) coupled analysis of electromechanical structures, previously used for the assessment of both 2D and 3D evaluations of the effective EMCCs [14]. Furthermore, a full 3D analysis of a CD-ROM drive base with shunted piezoelectric patches has previously been analyzed in ANSYS® [15], while the possibility of exporting system matrices and vectors has been further utilized in [16] to determine optimal shunt calibration and in [17] for optimal patch positioning by optimization functions written in Matlab. Presently, the implementation of the new shunt calibration method in ANSYS® is used to perform full 3D analysis of a benchmark problem concerning a simply supported plate presented in [6] with a single pair of piezoceramic patches and subsequently with multiple pairs placed symmetrically with respect to the targeted vibration forms. The aim of the paper is to introduce an adapted calibration procedure that is suitable for use and implementation in commercial FE software and consistently incorporates the effective EMCC to accurately represent the effects from non-resonant modes in a flexible structure.

2 Finite element formulation

This section is devoted to the notations and general structure of commercial codes with electromechanical packages, such as the ANSYS® 3D FE model, and is presented to clarify and support the theory behind the proposed shunt calibration procedure in [6] based on a consistent use of the effective EMCC.

2.1 Constitutive equations

The constitutive relations for piezoelectric materials can be written in four different forms, depending on the choice of independent variables. The most commonly implemented form in commercial software, such as ANSYS®, is the so-called e -form,

$$\{T\} = [C^E]\{S\} - [e]\{E\} \quad (1)$$

$$\{D\} = [e]^t\{S\} + [\epsilon^S]\{E\} \quad (2)$$

where superscript t denotes the transpose operation. For a full 3D representation, the six engineering stresses in $\{T\}$ and three electric displacements in $\{D\}$ are expressed in terms of the energy conjugated strains in $\{S\}$ and electric fields in $\{E\}$ through the SC elastic stiffness matrix $[C^E]$, piezoelectric (stress) coupling coefficients matrix $[e]$ and dielectric blocked constants matrix $[\epsilon^S]$. Details about the coupled constitutive relations in Eqs. (1)-(2) can be found in [14].

2.2 Eigenvalue equations

In the following, mechanically unloaded harmonic vibrations are considered by implying general harmonic solutions of the form $\{\dots\} = \{\dots\}e^{i\omega t}$, where ω is the representative angular frequency when t represents time. Thus, the variational formulation for the combined electromechanical structure can be written as

$$\int_{\Omega} \{\delta S\}^t \{T\} d\Omega - \omega^2 \int_{\Omega} \{\delta u\}^t \rho \{u\} d\Omega - \int_{\Omega} \{\delta E\}^t \{D\} d\Omega = \int_{\Gamma_q} \delta \phi q d\Gamma_q \quad (3)$$

where the δ indicates the variational function. In Eq. (3), ρ denotes the material mass density, ϕ the electric potential, q the corresponding surface charge density, Ω the material volume and Γ_q the area of the electrode where the charge q is applied or measured.

Upon substitution of the constitutive relations in Eqs. (1)-(2) into the variational equation (3), the stresses $\{T\}$ and electric displacements $\{D\}$ no longer appear explicitly in the variational equation (3). In the coupled FE formulation, the 3D displacements in the vector $\{u\}$ are then approximated by their nodal displacements in $\{U\}$ via appropriate shape functions, while a similar interpolation is used to represent the electric potential ϕ by the corresponding nodal values in $\{\varphi\}$. The corresponding mechanical strains in $\{S\}$ and electric fields in $\{E\}$ are then obtained by consistent differentiation of the shape functions associated with $\{U\}$ and $\{\varphi\}$, respectively. In the discrete representation by the nodal degrees of freedom (dofs), the variational equation (3) contains two coupled equations with system matrices obtained by performing the volume integration over Ω on the left hand side of Eq. (3) and the integral across the electrode area Γ_q on the right hand side. Hereby, the discrete vibrational problem can be represented by this coupled set of equations

$$\left(\begin{bmatrix} K_U^E & K_{U\varphi}^E \\ (K_{U\varphi}^E)^t & -K_{\varphi}^{\epsilon^S} \end{bmatrix} - \omega^2 \begin{bmatrix} M & 0 \\ 0 & 0 \end{bmatrix} \right) \begin{Bmatrix} U \\ \varphi \end{Bmatrix} = \begin{Bmatrix} 0 \\ -Q_{\varphi} \end{Bmatrix} \quad (4)$$

where $[K_U^E]$, $[K_{U\varphi}^E]$ and $[K_{\varphi}^{\epsilon^S}]$ contain the stiffness components associated with the mechanical displacements, electromechanical coupling and electric potentials, while M contains the physical mass associated with the vibrational inertia of the host structure and piezoelectric patches. Finally, the vector $\{Q_{\varphi}\}$ contains the applied electric charges from, for example, an external power source or a supplemental shunt.

When modelling a piezoelectric patch in an FE code, some dofs constitute the patch electrode, while other dofs describe the pure electromechanical material. A continuous electrode distributed on the patch is represented by a scalar electric potential via an equipotential condition, which in the present case is introduced for thin piezoceramic patches with two in-plane electrodes. In the case of a single patch or a single system of connected patches, only a single electric potential dof remains unconstrained once a non-wired (interface) electrode is grounded. Appendix A presents the extension to several independent pairs of symmetrically placed piezoceramic patches. When introducing the equipotential condition, the discrete vibrational problem (Eq. (4)) can be decomposed into

$$\left(\begin{bmatrix} K_U^E & \bar{K}_{U\varphi}^E & K_{UV}^E \\ (\bar{K}_{U\varphi}^E)^t & -\bar{K}_\varphi^{\epsilon^S} & -K_{\varphi V}^{\epsilon^S} \\ (K_{UV}^E)^t & -(K_{\varphi V}^{\epsilon^S})^t & -C_p^{\epsilon^S} \end{bmatrix} - \omega^2 \begin{bmatrix} M & 0 & 0 \\ 0 & 0 & 0 \\ 0 & 0 & 0 \end{bmatrix} \right) \begin{Bmatrix} U \\ \varphi \\ V \end{Bmatrix} = \begin{Bmatrix} 0 \\ 0 \\ -Q \end{Bmatrix} \quad (5)$$

While $[\bar{K}_{U\varphi}^E]$ and $[\bar{K}_\varphi^{\epsilon^S}]$ contain contributions associated with the electric potential dofs that are not part of an electrode, the coupling matrix $\{K_{UV}^E\}$ represents the apparent stiffness associated with the dofs representing the patch electrode and $C_p^{\epsilon^S}$ is the effective capacitance of the single network of piezoceramic patches. Thus, the electric potential on the ungrounded non-wired electrode defines the difference in electric potential or voltage V , while Q is the corresponding charge. Finally, $\{K_{\varphi V}^{\epsilon^S}\}$ describes the coupling between the non-electroded and the electroded dofs. The vibrational problem (Eq. (5)) may therefore be written in the collapsed format

$$\left(\begin{bmatrix} K^E & k_{me}^E \\ (k_{me}^E)^t & -\bar{C}_p^{\epsilon^S} \end{bmatrix} - \omega^2 \begin{bmatrix} M & 0 \\ 0 & 0 \end{bmatrix} \right) \begin{Bmatrix} U \\ V \end{Bmatrix} = \begin{Bmatrix} 0 \\ -Q \end{Bmatrix} \quad (6)$$

obtained by eliminating $\{\varphi\}$ from the second set of equations in Eq. (5). Hereby, the resulting system matrices and resulting modified capacitance follow as

$$[K^E] = [K_U^E] + [\bar{K}_{U\varphi}^E][\bar{K}_\varphi^{\epsilon^S}]^{-1}[\bar{K}_{U\varphi}^E]^t, \quad \bar{C}_p^{\epsilon^S} = C_p^{\epsilon^S} - \{K_{\varphi V}^{\epsilon^S}\}^t[\bar{K}_\varphi^{\epsilon^S}]^{-1}\{K_{\varphi V}^{\epsilon^S}\} \quad (7)$$

while the coupling between the mechanical and electric domains is computed as

$$\{k_{me}^E\} = \{K_{UV}^E\} - [\bar{K}_{U\varphi}^E][\bar{K}_\varphi^{\epsilon^S}]^{-1}\{K_{\varphi V}^{\epsilon^S}\} \quad (8)$$

It is found that the compact form of the equations of motion in Eq. (6) is equivalent to the system previously derived in [6] with a slightly different notation for the electromechanical coupling.

3 Electromechanical coupling coefficients

The vibrational problem (Eq. (6)) constitutes the governing equation used in the subsequent analysis and derivations, in which the mechanical and electric stiffnesses are governed by the stiffness matrix $[K^E]$ and the resulting capacitance in Eq. (7), while the coupling between the system of mechanical equations and the single electric equation is governed by the electromechanical coupling vector $\{k_{me}^E\}$ in Eq. (8). For a specific vibration mode of the structure, the magnitude of the electromechanical coupling is conveniently represented by the effective EMCC, basically describing the modal ratio between electrical and mechanical stiffnesses. In this section, the effective EMCC and its quasi-static approximation are derived and then subsequently used to calibrate resonant RL shunt circuits for optimal piezoelectric vibration damping.

3.1 Effective EMCC

The effective EMCC may be defined as the rate of converted energy by the piezoelectric material and therefore described by the difference between the modal strain energies associated with SC and OC patch electrodes. The modal strain energies are proportional to the eigenvalues from the SC and OC eigenvalue problems [14], obtained from Eq. (6) with $V = 0$ and $Q = 0$, respectively. For vanishing voltage, the SC eigenvalue problem can be directly written as

$$([K^E] - \omega_j^2[M]) \{U\}_j = \{0\} \quad (9)$$

for a particular vibration mode j with circular frequency ω_j . In the SC limit, the bottom equation in Eq. (6) provides the (sensed) modal charge

$$Q_j = -\{k_{me}^E\}^t \{U\}_j \quad (10)$$

as a reaction force securing $V = 0$. This modal charge is easily extracted from a FE solution and therefore conveniently used to determine the effective EMCC. The SC eigenvalue problem Eq. (9) conveniently constitutes the foundation of a dynamic analysis, with the mode shape vectors $\{U\}_j$ normalized to unit modal mass,

$$\{U\}_j^t [M] \{U\}_j = 1 \quad , \quad \{U\}_j^t [K^E] \{U\}_j = \omega_j^2 \quad (11)$$

while ω_j^2 then determines the corresponding modal stiffness.

The opposite OC eigenvalue problem follows from Eq. (6) for vanishing charge ($Q = 0$), conveniently formulated as

$$\left([K^E] + \frac{1}{\bar{C}_p^{\epsilon^S}} \{k_{me}^E\} \{k_{me}^E\}^t - \hat{\omega}_j^2 [M] \right) \{\hat{U}\}_j = \{0\} \quad (12)$$

to secure a non-vanishing determinant of the resulting mass matrix. In the corresponding stiffness matrix, the SC contribution $[K^E]$ is then increased by the quadratic projection of the coupling vector $\{k_{me}^E\}$ on the modified capacitance $\bar{C}_p^{\epsilon^S}$ such that the OC circular frequency $\hat{\omega}_j \geq \omega_j$. In the following the $(\hat{\cdot})$ -symbol denotes solutions for the OC configuration.

The calibration procedure is derived for a specific target mode $j = r$ with circular SC and OC frequencies ω_r and $\hat{\omega}_r$, respectively. The effective EMCC for this mode is referred to as κ_e^2 , representing the ability to convert between mechanical and electrical energy and therefore the damping attainable by the supplemental shunt. The effective EMCC is presently defined by the relative difference between the SC and OC circular frequencies squared,

$$\kappa_e^2 = \frac{\hat{\omega}_r^2 - \omega_r^2}{\omega_r^2} \quad (13)$$

Pre-multiplying Eq. (9) with $\{\hat{U}\}_r^t$ and oppositely Eq. (12) with $\{U\}_r^t$, the terms involving $[K^E]$ may be eliminated so that the effective EMCC for the target mode r can be expressed as

$$\kappa_e^2 = \frac{\{U\}_r^t \{k_{me}^E\} \{k_{me}^E\}^t \{\hat{U}\}_r}{\omega_r^2 \bar{C}_p^{\epsilon^S} \{U\}_r^t [M] \{\hat{U}\}_r} \quad (14)$$

A simpler expression is obtained by assuming $\{\hat{U}\}_r \simeq \{U\}_r$, which is commonly used in the literature [9]. Thus, the effective EMCC can be estimated as

$$\kappa_0^2 = \frac{Q_r^2}{\omega_r^2 \bar{C}_p^{\epsilon^S}} \quad (15)$$

whereby evaluation of the OC eigenvalue problem in Eq. (12) can be avoided.

3.2 Quasi-static EMCC

The approximation in Eq. (15) of the effective EMCC in Eq. (13) has in [6] been demonstrated to be rather imprecise for flexible host structures. However, a more accurate approximation can quite simply be obtained by considering two static problems associated with SC and OC patch electrodes, obtained from Eq. (6) when $[M] = [0]$ and a mechanical load $\{f\}$ is applied. As for the approximative solution in Eq. (15), this quasi-static approach avoids solving the OC eigenvalue problem in Eq. (12). When applying any external load to the electromechanical structure with SC patch electrodes the quasi-static solution to the measured charge is found as

$$Q_s = -\{k_{me}^E\}^t [K^E]^{-1} \{f\} \quad (16)$$

with subscript s referring to a sufficiently static limit where the inertia can be neglected. As the same external load $\{f\}$ is applied to the structure with OC electrodes, the deflection is slightly altered due to the electromechanical stiffening. This gives the following solution for the difference in electric potential between the patch electrodes for the quasi-static behaviour,

$$V_s = \frac{\{k_{me}^E\}^t [K^E]^{-1} \bar{C}_p^{\epsilon^S}}{1 + \{k_{me}^E\}^t [K^E]^{-1} \{k_{me}^E\} / \bar{C}_p^{\epsilon^S}} \{f\} \quad (17)$$

Note that the inverse of the SC stiffness matrix is obtained explicitly by the Sherman-Morrison relation [18]. Both the quasi-static solution to the measured charge Q_s and the difference in electric potential V_s are easily accessible reaction and response outputs in any electromechanical FE analysis, from which the quasi-static capacitance of the piezoceramic patches can be evaluated as

$$C_s = -\frac{Q_s}{V_s} = \bar{C}_p^{\epsilon^S} + \{k_{me}^E\}^t [K^E]^{-1} \{k_{me}^E\} \quad (18)$$

This quasi-static capacitance C_s is more precise than the modified capacitance $\bar{C}_p^{\epsilon^S}$ since it includes the (static) interaction with the specific host structure by the last term in Eq. (18). This further implies an improved approximation of the effective EMCC ($\kappa_e^2 \simeq \kappa_s^2$) by an expression similar to Eq. (15)

$$\kappa_s^2 = \frac{Q_r^2}{C_s \omega_r^2} \quad (19)$$

where $\bar{C}_p^{\epsilon^S}$ has been replaced by C_s . The use of the quasi-static EMCC in Eq. (19) might be a suitable alternative in both practical applications and experiments when the SC and OC natural frequencies are almost indistinguishable. Furthermore, for large and complex FE models this method may require less computational effort than solving the dynamic eigenvalue problems.

4 Modal reduced equations

A reduced order model for the vibrating structure is effectively introduced by a modal representation in terms of the most energetic vibration form. In this section, the representative modal equations are derived in order to obtain an accurate shunt tuning method that is suitable for implementation in a commercial FE-software. The structural part of Eq. (6) is effectively described by the mode shapes $\{U\}_j$ from the SC limit, collected as columns in the modal matrix $[U]$. Hereby, the structural response $\{U\}$ in Eq. (6) can be represented as

$$\{U\} = [U]\{v\} \quad (20)$$

where the vector $\{v\}$ contains the modal coordinates. When substituting Eq. (20) into Eq. (6) and then pre-multiplying the structural equation with the vibration form $\{U\}_r^t$ of the resonant mode $j = r$, the coupled set of modal equations can be written as

$$(\omega_r^2 - \omega^2)v_r = Q_r V \quad (21)$$

$$\bar{C}_p^{\epsilon^S} V - Q = -\{Q\}^t \{v\} \quad (22)$$

where the vector $\{Q\}^t = \langle Q_1, Q_2 \dots \rangle$ contains the modal sensed charges Q_j defined in Eq. (10). Thus, the right hand side of Eq. (22) contains contribution from both the resonant mode through the modal charge Q_r as well as residual contributions from the non-resonant modes due to the non-vanishing Q_j for $j \neq r$. The residual terms ($j \neq r$) are now represented by two supplemental terms that are proportional to the electrical forcing V and describe corrections to the system impedances. Thus, the right hand side of Eq. (22) is approximated as

$$\{Q\}^t \{v\} = Q_r v_r + \left(C_r' - \frac{1}{\omega^2 L_r'} \right) V \quad (23)$$

where C_r' and L_r' are artificial capacitance and inductance, respectively, taking into account the influence from the non-resonant structural modes ($j \neq r$). The two correction terms can be calculated explicitly and elegantly based on the system matrices [5]. However, next, the correction terms are instead calibrated by solving three eigenvalue problems associated with SC and OC patch electrodes and a pure inductive shunt with an optimally tuned inductance from the preferred calibration formulae without residual mode corrections. Elimination of $Q_r v_r$ between Eqs. (21)-(23) gives the governing equation

$$\left[\left(\bar{C}_p^{\epsilon^S} + C_r' - \frac{1}{\omega^2 L_r'} \right) (\omega_r^2 - \omega^2) + Q_r^2 \right] V = Q (\omega_r^2 - \omega^2) \quad (24)$$

where the relation between charge Q and voltage V depends on the particular shunt impedance.

4.1 SC and OC electrodes

The SC condition corresponds to $V = 0$, in which case the non-trivial solution to Eq. (24) is readily obtained as $\omega = \omega_r$, exactly recovering the solution to the SC eigenvalue problem in Eq. (9). The corresponding OC condition follows when $Q = 0$ and the associated circular frequency $\hat{\omega}_r$ may be obtained numerically from Eq. (12) or experimentally by measurements. The relative difference between the SC and OC frequencies defines the effective EMCC by the relation in Eq. (13). Thus, substituting the OC frequency $\omega = \hat{\omega}_r$ into Eq. (24) and then imposing $Q = 0$, the former becomes

$$\left[\left(C_r - \frac{1}{\hat{\omega}_r^2 L_r'} \right) (\omega_r^2 - \hat{\omega}_r^2) + Q_r^2 \right] V = 0 \quad (25)$$

after introducing

$$C_r = \bar{C}_p^{\epsilon^S} + C_r' \quad (26)$$

as a modal capacitance, modified by the quasi-static correction term C_r' introduced in Eq. (23). Solving for non-trivial solutions with $V \neq 0$, the problem in Eq. (25) constitutes a quadratic equation in $\hat{\omega}_r^2$. The effective EMCC κ_e^2 can thereby be obtained from the solution to this quadratic equation, see details in Appendix B, as

$$\kappa_e^2 = \frac{\hat{\omega}_r^2 - \omega_r^2}{\omega_r^2} = \kappa_r^2 + \frac{1}{2} (1 + \kappa_r^2 - \lambda_r' \kappa_r^2) \left(\sqrt{1 + \frac{4(\kappa_r^2)^2 \lambda_r'}{(1 + \kappa_r^2 - \lambda_r' \kappa_r^2)^2}} - 1 \right) \quad (27)$$

in which the inertia correction from the residual modes is represented by

$$\lambda'_r = \frac{1}{Q_r^2 L'_r} \quad (28)$$

while the flexibility correction in C_r is contained in a modified EMCC (see Eqs. (15) and (26))

$$\kappa_r^2 = \frac{Q_r^2}{C_r \omega_r^2} \quad (29)$$

It follows from Eq. (27) that for vanishing inertia correction from the residual modes ($\lambda'_r = 0$), the modified EMCC is $\kappa_r^2 = \kappa_e^2$. And if furthermore the flexibility correction is ignored ($C'_r = 0$), the modal capacitance $C_r = \bar{C}_p^{\epsilon^S}$ and the EMCC $\kappa_e^2 = \kappa_0^2$ from Eq. (15).

An improved estimate is achieved for finite $\lambda'_r \ll 1$, whereby a Taylor expansion of first order can be applied on the square root in Eq. (27). This gives

$$\kappa_e^2 = \kappa_r^2 \frac{1 + \kappa_r^2}{1 + \kappa_r^2 - \lambda'_r \kappa_r^2} = \frac{Q_r^2}{C_L \omega_r^2} \quad (30)$$

where the latter equality defines an actual modal capacitance C_L of the piezoelectric patches around the targeted resonance $j = r$,

$$C_L = C_r \left(1 - \frac{\lambda'_r \kappa_r^2}{1 + \kappa_r^2} \right) \quad (31)$$

It is found that for vanishing λ'_r the inertia reduced capacitance C_r recovers the actual capacitance C_L associated with κ_e^2 .

It follows from Eq. (30) that the effective EMCC is the ratio between the apparent electrical absorber stiffness Q_r^2/C_L and the modal stiffness ω_r^2 . The expression in Eq. (30) can furthermore be used to determine the artificial inductance L'_r as

$$\frac{1}{(1 + \kappa_r^2) \omega_r^2 L'_r} = \left(1 - \frac{\kappa_r^2}{\kappa_e^2} \right) \frac{Q_r^2}{\kappa_r^2 \omega_r^2} \quad (32)$$

using Eqs. (28) and (31). By elimination of L'_r , using Eqs. (32), (26) and (29), the governing modal equation (24) can be expressed as

$$\left\{ \left[\frac{\omega^2}{\omega_r^2} - (1 + \kappa_r^2) \left(1 - \frac{\kappa_r^2}{\kappa_e^2} \right) \right] \left(1 - \frac{\omega^2}{\omega_r^2} \right) + \kappa_r^2 \frac{\omega^2}{\omega_r^2} \right\} V = \frac{Q}{Q_r^2} \kappa_r^2 \omega^2 \left(1 - \frac{\omega^2}{\omega_r^2} \right) \quad (33)$$

containing both the effective EMCC κ_e^2 and the modified EMCC κ_r^2 .

As mentioned above, a simplified representation can be obtained by assuming that $L'_r \rightarrow \infty$, whereby the last (inertia) correction term in Eq. (23) vanishes, leaving only the former flexibility term proportional to C'_r . For this approximation, it follows directly from Eq. (27) that $\kappa_r^2 = \kappa_e^2$, obtained directly from Eq. (13). The validity and accuracy of $\kappa_r^2 = \kappa_e^2$ is verified by the numerical results obtained in Section 7 and the tuning formulae presented in Section 5 which are therefore expressed directly in terms of κ_e^2 . However, for a non-negligible residual mode inertance, represented by L'_r , a supplemental condition is then needed to separate the individual correction effects from C'_r and L'_r . This separation is conveniently achieved by introducing a pure inductive (L) shunt that creates a supplemental resonance. For completeness, this improved L -shunt calibration is now summarized, although its influence is limited for most flexible structures, as illustrated in [6].

4.2 Pure L -shunt

In the OC limit, the effective EMCC κ_e^2 in Eq. (27) or Eq. (30) depends on both the flexibility correcting capacitance C'_r in κ_r^2 and the inertia correcting inductance L'_r in λ'_r . In order to distinguish these two non-resonant modal corrections, a supplemental condition must be introduced. By introducing a pure inductive (L) shunt, an expression for κ_r^2 can be determined by solving the corresponding quadratic characteristic equation, as detailed subsequently.

For a pure L -shunt, the impedance relation between charge and voltage can be written as

$$V = \omega^2 L Q \quad (34)$$

Hereby, the charge Q can be eliminated, after using Eq. (34), in Eq. (33), whereby the characteristic equation associated with $V \neq 0$ can be written as

$$\left(\frac{\omega}{\omega_r}\right)^4 - \left[1 + \kappa_r^2 + (1 + \kappa_r^2) \left(1 - \frac{\kappa_r^2}{\kappa_e^2}\right) + \lambda_r \kappa_r^2\right] \left(\frac{\omega}{\omega_r}\right)^2 + (1 + \kappa_r^2) \left(1 - \frac{\kappa_r^2}{\kappa_e^2}\right) + \lambda_r \kappa_r^2 = 0 \quad (35)$$

representing the shunt inductance L in normalized form as

$$\lambda_r = \frac{1}{Q_r^2 L} \quad (36)$$

similar to Eq. (28) for the correction inductance L'_r . It is noted that the form of λ_r in Eq. (36) is due to the present normalization of the SC mode shapes to unit modal masses in Eq. (11).

Because of the inclusion of the inductance L , the quadratic characteristic equation (35) governs two roots ω_-^2 and ω_+^2 , with the corresponding circular frequencies ω_- and ω_+ being smaller and larger than the SC circular frequency ω_r , respectively. The two circular frequencies associated with the L -shunt can be found experimentally or numerically by solving the eigenvalue problem Eq. (6) with Q eliminated by Eq. (34),

$$\left(\begin{bmatrix} K^E & k_{me}^E \\ 0 & 1 \end{bmatrix} - \omega^2 \begin{bmatrix} M & 0 \\ -(k_{me}^E)^t L & \bar{C}_p^{\epsilon^S} L \end{bmatrix}\right) \begin{Bmatrix} U \\ V/L \end{Bmatrix} = \begin{Bmatrix} 0 \\ 0 \end{Bmatrix} \quad (37)$$

The product of the two roots must be equal to the constant term in Eq. (35), which gives the condition

$$\left(\frac{\omega_+}{\omega_r}\right)^2 \left(\frac{\omega_-}{\omega_r}\right)^2 = \lambda_r^* \kappa_r^2 \quad (38)$$

where

$$\lambda_r^* = \frac{1 + \kappa_r^2}{\kappa_r^2} \left(1 - \frac{\kappa_r^2}{\kappa_e^2}\right) + \lambda_r \quad (39)$$

represents the κ_r^2 factored out constant term in the characteristic equation (35). It may be noted, considering the first relation of Eq. (30), that $\lambda_r^* = \lambda'_r + \lambda_r$ represents the combined inductance from shunt, Eq. (36) and residual modes Eq. (28).

The sum of roots must further equal the coefficient to the linear term in Eq. (35) with opposite sign, which results in

$$\left(\frac{\omega_+}{\omega_r}\right)^2 + \left(\frac{\omega_-}{\omega_r}\right)^2 = 1 + \kappa_r^2 (1 + \lambda_r^*) \quad (40)$$

Subtracting Eq. (38) from Eq. (40) gives the modified EMCC as

$$\kappa_r^2 = \left(1 - \frac{\omega_-^2}{\omega_r^2}\right) \left(\frac{\omega_+^2}{\omega_r^2} - 1\right) \quad (41)$$

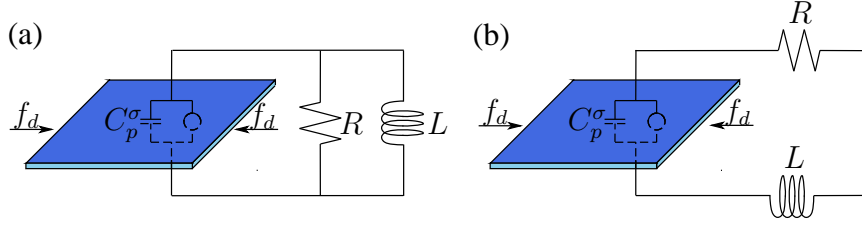


Figure 1: (a) Parallel and (b) series shunted piezoceramic patch with inherent capacitance C_p^σ .

Once κ_r^2 is determined, the modal capacitance C_r is obtained from Eq. (29), whereby the quasi-static correction capacitance C_r' subsequently follows from Eq. (26) after using Eq. (15), as

$$C_r' = C_r - \bar{C}_p^{\epsilon^S} = \left(1 - \frac{\kappa_r^2}{\kappa_0^2}\right) \frac{Q_r^2}{\kappa_r^2 \omega_r^2} \quad (42)$$

The corresponding inductive correction term L_r' is determined by the previously derived expression in Eq. (32).

The introduction of the pure L -shunt enables the individual determination of the two correction terms in Eq. (23) with the artificial modal capacitance C_r' and inductance L_r' . However, in the following, the modified EMCC κ_r^2 is replaced by the effective EMCC κ_e^2 , which is readily available from an FE analysis when using the definition in Eq. (14). As demonstrated in the present section, this estimate of κ_e^2 is valid for vanishing λ_r' .

5 Resonant shunt tuning

The resonant shunt circuit consists of an inductance L and a resistance R connected either in parallel or in series, as shown in Figure 1. For both circuit connections, the charge Q on the right hand side of Eq. (33) can be eliminated by the generalised Ohm's law

$$V = -i\omega Z_{sh}(\omega)Q \quad (43)$$

where $Z_{sh}(\omega)$ is the impedance of the supplemental shunt.

Upon elimination, by Eq. (43), of Q in Eq. (33), the corresponding characteristic equation can be written as

$$\left[\frac{\omega^2}{\omega_r^2} - (1 + \kappa_r^2) \left(1 - \frac{\kappa_r^2}{\kappa_e^2}\right) - i\omega \frac{1}{Z_{sh}(\omega) Q_r^2 \kappa_r^2} \right] \left(1 - \frac{\omega^2}{\omega_r^2}\right) + \kappa_r^2 \frac{\omega^2}{\omega_r^2} = 0 \quad (44)$$

Next, the calibration principle for the parallel and series RL resonant shunt circuits are considered, in which the tuning expressions are subsequently simplified by assuming $\kappa_r^2 \simeq \kappa_e^2$.

5.1 Parallel shunt circuit

The schematics of a parallel shunted piezoceramic patch is shown in Figure 1(a). Because of its inductive property it operates as a vibration absorber on the host structure and details about its equivalent mechanical properties are provided in [1]. The impedance $Z_{sh}(\omega)$ is for the parallel shunt circuit given as

$$\frac{1}{Z_{sh}(\omega)} = \frac{1}{R} + \frac{1}{i\omega L} \quad (45)$$

and, by substituting the latter into Eq. (44), the characteristic equation can be written as

$$\left(\frac{\omega}{\omega_r}\right)^4 - \left(1 + \kappa_r^2 + \lambda_r^* \kappa_r^2\right) \left(\frac{\omega}{\omega_r}\right)^2 + \lambda_r^* \kappa_r^2 + i \left(\frac{\omega}{\omega_r}\right) \rho_r^p \kappa_r^2 \omega_r \left[1 - \left(\frac{\omega}{\omega_r}\right)^2\right] = 0 \quad (46)$$

where the electric damping parameter (superscript p refers to *parallel*)

$$\rho_r^p = \frac{1}{RQ_r^2} \quad (47)$$

is inversely proportional to the shunt resistance R . Furthermore, the shunt inductance L is contained in λ_r^* as defined in Eq. (39), with the normalized shunt inductance λ_r introduced in Eq. (36).

When introducing the estimate $\kappa_r^2 \simeq \kappa_e^2$, the characteristic equation Eq. (46) reduces to

$$\left(\frac{\omega}{\omega_r}\right)^4 - \left(1 + \kappa_e^2 + \lambda_r \kappa_e^2\right) \left(\frac{\omega}{\omega_r}\right)^2 + \lambda_r \kappa_e^2 + i \left(\frac{\omega}{\omega_r}\right) \rho_r^p \kappa_e^2 \omega_r \left[1 - \left(\frac{\omega}{\omega_r}\right)^2\right] = 0 \quad (48)$$

where λ_r then directly replaces λ_r^* from Eq. (39). In the following Eq. (48) constitutes the basis of the shunt tuning.

Initially, the tuning of the inductance L in λ_r must secure that the electric shunt reacts properly in resonance with the targeted mode $j = r$. For this, the principle of equal modal damping is applied; initially, the latter was introduced for the mechanical tuned mass damper in [19] and subsequently proposed for pole placement calibration of a resonant series RL shunt [1]. The principle states that the two complex roots must meet at a bifurcation point, whereby they have equal damping up to the point of bifurcation because the roots follow semi-circular trajectories for increasing ρ_r^p . It, furthermore, implies that equal damping can be secured for a pure L -shunt in the limit $\rho_r^p \rightarrow 0$, at which the real-valued roots ω_- and ω_+ must be inverse points with respect to the circular frequency ω_r in the opposite (SC) limit $\rho_r^p \rightarrow \infty$. For $\rho_r^p \rightarrow 0$, the characteristic equation (46) recovers Eq. (35) for the pure L -shunt. The inverse point condition can therefore be directly represented by the relation $\lambda_r \kappa_e^2 = 1$, see Eq. (48). Hereby, the inductance calibration follows readily from Eq. (36) as

$$L = \frac{\kappa_e^2}{Q_r^2} \quad (49)$$

It is important to observe that the optimal inductance is given by the effective EMCC κ_e^2 relative to the square of the modal charge Q_r in Eq. (10), obtained directly from an FE analysis as a reaction force associated with the SC eigenvalue problem.

In Figure 2(a), the blue trajectories represent the path of the complex roots in the first quadrant, obtained by solving the characteristic equation Eq. (46) with respect to ρ_r^p as gain. For infinite resistance ($\rho_r^p \rightarrow 0$), the roots recover ω_- and ω_+ below and above ω_r . When increasing ρ_r^p (or decreasing the resistance), the two roots move into the complex plane along semi-circular paths until they meet at the bifurcation point, whereafter one root becomes heavily damped when approaching the imaginary axis along a quarter circle, while the other root becomes undamped when terminating at the SC solution ω_r for $\rho_r^p \rightarrow \infty$. Thus, the reference frequency for the parallel RL shunt is associated with the SC configuration.

The shunt resistance is now tuned to secure a reasonably flat plateau in the frequency response curve. Several expressions have been proposed for this calibration [3, 4, 8] and in the present

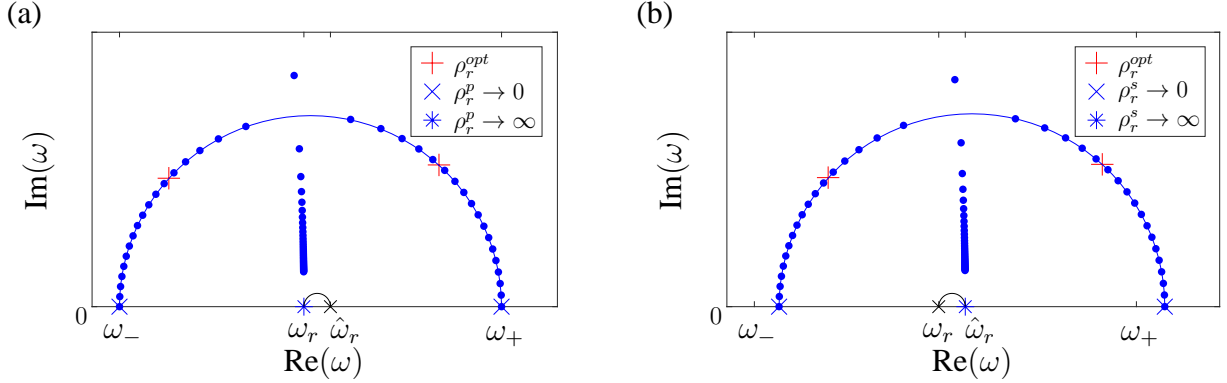


Figure 2: Root-Locus diagram for (a) parallel Eq. (46) and (b) series Eq. (52) shunt circuits.

Table 1: Tuning procedure based on the effective EMCC for parallel and series shunt circuits with $\kappa_r^2 \simeq \kappa_e^2$.

Parallel		Series	
$L = \frac{\kappa_e^2}{Q_r^2}$	$R = \frac{\kappa_e^2 \omega_r}{Q_r^2} \sqrt{\frac{1}{2\kappa_e^2}}$	$L = \frac{\kappa_e^2}{Q_r^2 (1 + \kappa_e^2)^2}$	$R = \frac{\kappa_e^2 \omega_r}{Q_r^2} \sqrt{\frac{2\kappa_e^2}{(1 + \kappa_e^2)^3}}$

case the resistance tuning in [1, 13, 19, 20]. By comparing the generic equation (33) in [20] with the characteristic equation (48), this gives the optimum resistance tuning as

$$R = \frac{\kappa_e^2 \omega_r}{Q_r^2} \sqrt{\frac{1}{2\kappa_e^2}} \quad (50)$$

when the approximation $\kappa_r^2 \simeq \kappa_e^2$ has been introduced. The tuning in Eq. (50) provides a reasonable compromise between large modal damping and effective response mitigation, and furthermore it gives a flat plateau in the amplitude curve for the shunt loading V . The complex roots obtained by Eq. (50) are indicated by the red crosses in Figure 2(a).

As demonstrated in [13], it is numerically advantageous and, for most actual problems, sufficiently accurate to base the tuning of the resistance on the effective EMCC, whereby $\kappa_r^2 \simeq \kappa_e^2$ is used in the calibration formulae for both L and R . Thus, the subsequent implementation of the shunt tuning method only involves the use of modal parameters ω_r , Q_r and κ_e^2 for the SC and OC configurations, while avoiding the pure L -shunt and its supplemental eigenvalue problem in Eq. (37). The tuning formulae for the parallel shunt are summarized in Table 1.

5.2 Series shunt circuit

The series shunted piezoceramic patch is shown in Figure 2(b). This configuration implies that the residual mode corrections and shunt components are not additive, whereby optimal calibration is associated with an iterative procedure, unless the assumption $\kappa_r^2 \simeq \kappa_e^2$ is conveniently introduced, as demonstrated subsequently.

The series shunt impedance is introduced as

$$Z_{sh}(\omega) = R + i\omega L \quad (51)$$

whereby substitution into Eq. (44) gives this characteristic equation (see Appendix C for its

derivation)

$$\begin{aligned} \left(\frac{\omega}{\hat{\omega}_r}\right)^4 - \left(\frac{1 + \kappa_r^2}{1 + \kappa_e^2} + \frac{\lambda_r^* \kappa_r^2}{1 + \kappa_e^2}\right) \left(\frac{\omega}{\hat{\omega}_r}\right)^2 + \frac{\lambda_r^* \kappa_r^2}{(1 + \kappa_e^2)^2} \\ + i \left(\frac{\omega}{\hat{\omega}_r}\right) \rho_r^s \frac{\lambda_r}{\hat{\omega}_r} \left\{ \frac{1 + \kappa_r^2}{1 + \kappa_e^2} - \left(\frac{\omega}{\hat{\omega}_r}\right)^2 + \frac{1 + \kappa_r^2}{1 + \kappa_e^2} \left(1 - \frac{\kappa_r^2}{\kappa_e^2}\right) \left[\left(\frac{\omega_r}{\omega}\right)^2 - 1\right] \right\} = 0 \end{aligned} \quad (52)$$

conveniently given in terms of the OC frequency $\hat{\omega}_r$ and introduction of an electric damping parameter (superscript s refers to series)

$$\rho_r^s = RQ_r^2 \quad (53)$$

that becomes proportional to the shunt resistance R .

In Eq. (52), the characteristic equation is actually quintic, due to the presence of the frequency ratio ω_r^2/ω^2 in the final term. However, by applying the estimate $\kappa_r^2 \simeq \kappa_e^2$ the last term inside the latter curled brackets vanishes and Eq. (52) reduces, after Eq. (39), to

$$\left(\frac{\omega}{\hat{\omega}_r}\right)^4 - \left(1 + \frac{\lambda_r \kappa_e^2}{1 + \kappa_e^2}\right) \left(\frac{\omega}{\hat{\omega}_r}\right)^2 + \frac{\lambda_r \kappa_e^2}{(1 + \kappa_e^2)^2} + i \left(\frac{\omega}{\hat{\omega}_r}\right) \rho_r^s \frac{\lambda_r}{\hat{\omega}_r} \left[1 - \left(\frac{\omega}{\hat{\omega}_r}\right)^2\right] = 0 \quad (54)$$

For this reduced equation, the desired inverse point relation is secured by $\lambda_r \kappa_e^2 = (1 + \kappa_e^2)^2$, corresponding to the roots ω_- and ω_+ for vanishing ρ_r^s being inverse points with respect to the OC natural frequency $\hat{\omega}_r$. The optimal inductance is then determined from Eq. (36) as

$$L = \frac{\kappa_e^2}{Q_r^2(1 + \kappa_e^2)^2} \quad (55)$$

For the inductance tuning in Eq. (55), the complex roots obtained by solving Eq. (52) are plotted in Figure 2(b) for increasing ρ_r^s . The root locus diagram verifies that ω_- and ω_+ are in fact inverse points on the real axis with respect to $\hat{\omega}_r$, whereby the OC natural frequency is the apparent reference frequency for the series RL shunt, as also observed by [11].

It can be seen from Figure 2(b) that the roots to Eq. (52) approximately follow a semi-circle in the complex plane up to a bifurcation point. However, due to the approximations associated with the inverse point relation, the bifurcation point is not perfectly met. The optimal resistance tuning indicated by red crosses in Figure 2(b) is again found by the balanced calibration devised in [20] by comparing its generic equation (33) with Eq. (54), which results in the resistance formula

$$R = \frac{\kappa_e^2 \hat{\omega}_r}{Q_r^2(1 + \kappa_e^2)^2} \sqrt{2\kappa_e^2} = \frac{\kappa_e^2 \omega_r}{Q_r^2} \sqrt{\frac{2\kappa_e^2}{(1 + \kappa_e^2)^3}} \quad (56)$$

expressed in terms of $\kappa_r^2 \simeq \kappa_e^2$. Thus, the optimum piezoelectric shunt tuning for both the parallel and series RL shunts are now consistently derived with respect to the SC modal charge Q_r , the SC circular frequency ω_r and the effective EMCC κ_e^2 obtained by the classical expression in Eq. (13). The calibration formulae used in the following numerical analysis are summarized in the second column of Table 1 for the series shunt connection.

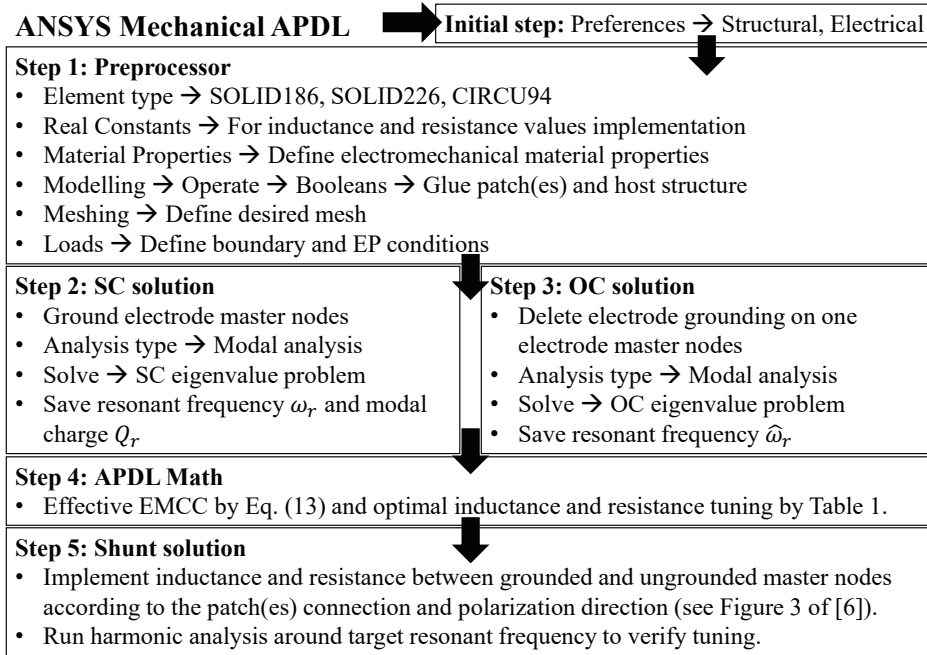


Figure 3: Flow chart illustrating ANSYS® implementation of the proposed optimum shunt tuning procedure.

6 Numerical implementation in ANSYS®

The modelling of the electromechanical structure in ANSYS®, evaluations of the SC and OC eigenvalue problems and implementation of the proposed shunt tuning method are summarized in the flow-chart shown in Figure 3, and briefly explained in the following. Initially, 'Structural' and 'Electrical' analyses have to be chosen. The first step then follows by defining the geometry, material properties, element types and mesh partitions of the analysed electromechanical structure. In the present work, SOLID186 and SOLID226 3D 20 node elements are used for the discretization of the host structure and piezoceramic patch(es), respectively. Next, the boundary conditions and equipotential (EP) conditions for all continuous electrodes are imposed to the discretized model. For each continuous electrode, the EP condition is defined in a master node which is saved for later use. In the second step, zero electric potential is applied to the master nodes to obtain SC piezoceramic patch(es). A modal analysis is then conducted to determine the targeted SC resonant frequency ω_r and modal charge Q_r , with the latter being a reaction force of the modal analysis. The third step deletes the zero electric potential constraint on one of the master nodes to obtain OC piezoceramic patch(es). A modal analysis is then conducted to determine the target OC resonant frequency $\hat{\omega}_r$. The fourth step then determines the effective EMCC κ_e^2 using Eq. (13), whereby the optimum inductance and resistance values can be determined according to Table 1 for either the parallel or series shunt circuit. The fifth and final step implements the optimum inductance and resistance between the grounded and ungrounded master nodes according to the patch(es) connection and polarization directions, see [6]. The inductance and resistance are implemented using CIRCU94 elements with specific key options and real constants. The shunt tuning can then be validated by performing a harmonic analysis around the target resonant frequency.

If the alternative tuning method based on the quasi-static EMCC κ_s^2 is preferred, the evaluation of the OC eigenvalue problem can be omitted, while two static problems associated with SC and

Table 2: Dimensions of simply supported plate with a single pair of piezoceramic patches.

Plate				Center patch	Piezoceramic PZT 5H
Dimensions $l_x \times l_y \times t$ [mm ³]	Density (kg/m ³)	Young's Modulus [GPa]	Poisson's ratio (-)	x,y [mm]	Dimensions $l_{px} \times l_{py} \times t_p$ [mm ³]
$414 \times 314 \times 1$	2700	70	0.33	$\frac{13}{28}l_x, \frac{15}{28}l_y$	$82.8 \times 62.8 \times 0.5$

OC patch electrodes must instead be solved. Finally, for single mode tuning with the effective EMCC approximated by the modal EMCC κ_0^2 in Eq. (15), the resulting modified capacitance is determined by Eq. (7b). In the following the performance of these three tuning methods are analysed for the smart plate benchmark [6] with either a single pair or four pairs of piezoceramic patches.

7 Benchmark examples

In the present section, the smart plate benchmark analysed in [6] is modelled with 3D FEs in ANSYS® with the aim of determining the optimum parallel and series shunt tuning and demonstrate the simplicity of the proposed tuning method based on ω_r , Q_r and κ_e^2 . Details about the dimensions of the simply supported plate and the single pair of piezoceramic patches as well as the location of the latter are provided in Table 2, along with the material properties of the plate. In the present work, it is chosen to use the piezoceramic material PZT 5H, for which the material properties can be accessed through the 'eFunda portal' [21].

7.1 Simply supported plate with a single pair of patches

The first example concerns optimum shunt tuning to the first eight vibration modes of the simply supported plate described in [6] with a single pair of piezoceramic patches. Initially, a short convergence study is carried out in order to justify the chosen discretization. It is first of all noted that increasing the number of elements in thickness direction only slightly alters the numerical results. The convergence study is thus carried out for an increasing number of elements along the two in-plane axes. The convergence of the squared SC and OC frequencies and effective EMCC for three of the first eight vibration modes is shown in Figure 4. The three modes 1, 4 and 7 are of particular interest because they possess significant electromechanical coupling, as indicated by large κ_e^2 in the following. The relative errors are obtained by comparing the approximate (approx) results to the reference (ref) ones obtained with a very fine mesh consisting of 23104 elements and 633064 dofs.

It can be seen from Figure 4(a) that the squared SC and OC frequencies converge rapidly and have relative errors below 1% (dashed black line) when using a model with approximately 10^4 dofs. Further, a nearly linear tendency of the convergence on the double logarithmic scale can be observed, indicating quadratic convergence. From Figure 4(b) it can be seen that the convergence of the squared effective EMCC is slower than that for the SC and OC frequencies. This is because κ_e^2 is determined as the relative difference between $\hat{\omega}_r^2$ and ω_r^2 , where the SC frequency simply converges faster than the OC one. It is seen that the relative error on the effective EMCC is around 1% (dashed black line) when using a model with approximately 1.5×10^5 dofs. This discretization is therefore used in the present analysis. The relative error on the effective EMCC for the remaining five vibration modes might be larger since the convergence rate is proportional to the magnitude of κ_e^2 , as demonstrated in [14].

The first eight vibration modes for the simply supported plate with a single SC pair of piezoceramic patches are shown in Figure 5, with the location of the patch pair indicated by the

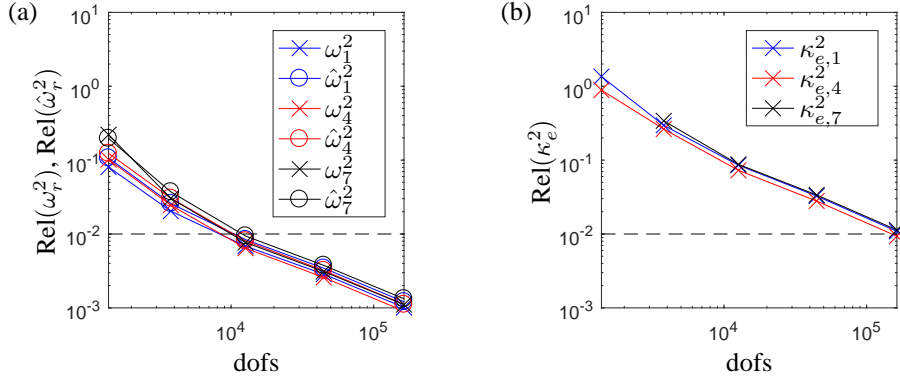


Figure 4: Convergence of (a) SC and OC frequencies and (b) effective EMCC for modes 1, 4 and 7, determined by $\text{Rel}(X)[\%] = (X_{\text{approx}} - X_{\text{ref}})/X_{\text{ref}}$.

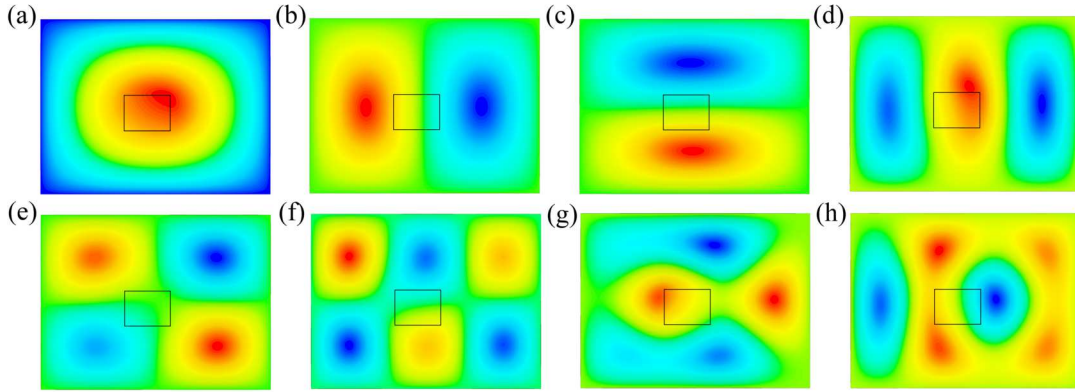


Figure 5: Mode shapes of a simply supported plate with a single SC patch pair.

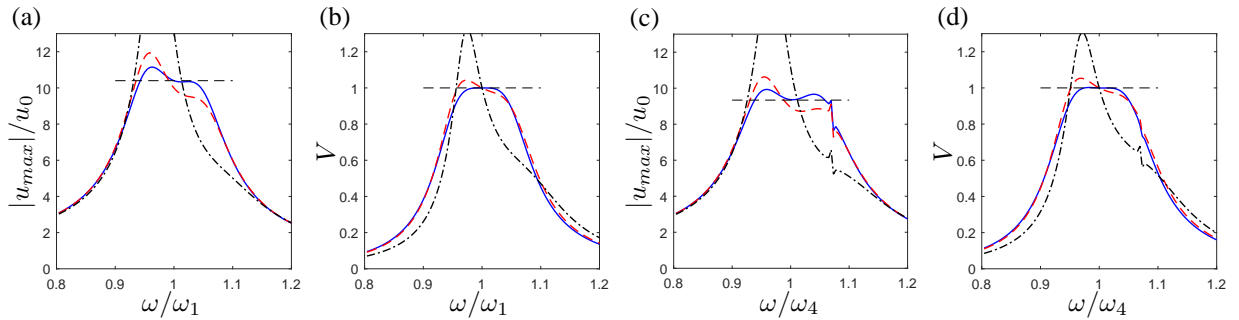
black rectangle. It can be seen from Figure 5(a,d,g) that the pair of piezoceramic patches is favourably positioned targeting vibration modes 1, 4 and 7, as their large curvatures over the patch area give large in-plane patch deformation. For the remaining five vibration modes, the pairs are positioned close to nodal points, whereby the EP condition results in cancellation of the charge across the patch area.

Table 3 provides the SC and OC frequencies, the effective EMCC, the normalized modal charge and the optimum parallel (p) and series (s) shunt tunings for modes 1 to 8. It can be seen for the present piezoceramic patch design that damping with the present patch pair location and dimensions is attainable for modes 1, 4 and 7, denoted in bold face in Table 3. The squared effective EMCCs are for these three modes around 2%, yielding a damping ratio of approximately $\zeta_{1,4,7} = \sqrt{\frac{1}{8}\kappa_e^2} \approx 5\%$, see [1]. It is seen that the normalized modal charge Q_r is seemingly proportional to the level of attainable damping. Finally, it is noted in Table 3 that the parallel and series optimum inductances have the same order of magnitude, while much lower resistance values are required for the series shunt configuration.

The tuning of the electronic components could as well have been based on the quasi-static (Eq. (19)) or the modal (Eq. (15)) EMCC, whereby evaluation of the OC eigenvalue is avoided. For the quasi-static EMCC, the two static Eqs. (16) and (17) must instead be computed, whereby the quasi-static capacitance can be determined by Eq. (18). In the present example, this is found to

Table 3: SC and OC frequencies, effective EMCC, normalized modal charge and optimum RL -shunt tunings, for simply supported plate with a pair of same poled and parallel wired piezoceramic patches.

Mode (type)	f [Hz]	\hat{f} [Hz]	κ_e^2 [%]	$Q_r^2/\omega_r^2 \left[\mu \left(\frac{C_s}{r_{ad}} \right)^2 \right]$	L_p [H]	R_p [k Ω]	L_s [H]	R_s [k Ω]
1 (1,1)	35.89	36.22	1.86	1.013	36.03	42.16	34.73	1.523
2 (2,1)	80.73	80.77	0.10	0.054	7.071	80.96	7.057	0.159
3 (1,2)	111.9	112.0	0.12	0.066	3.604	52.32	3.592	0.122
4 (3,1)	154.7	156.5	2.30	1.252	1.943	8.810	1.857	0.392
5 (2,2)	165.7	165.7	0.02	0.008	1.999	1.115	1.998	0.038
6 (3,2)	230.6	230.7	0.04	0.027	0.744	37.31	0.744	0.031
7 (1,3)	242.3	244.8	2.01	1.067	0.814	6.176	0.782	0.241
8 (4,1)	252.3	252.3	0.00	0.000	0.976	24.17	0.976	0.010


Figure 6: FRP for displacement and voltage around the (a)+(b) first and (c)+(d) fourth resonant frequency for parallel shunt tuning based on the effective Eq. (13) (solid line), quasi-static Eq. (19) (dashed line) and modal Eq. (15) (dashed-dotted line) EMCC in respect to mode r .

be $C_s = 554.6\text{nF}$. The quasi-static EMCC κ_s^2 then follows by multiplying the inverse of C_s with Q_r^2/ω_r^2 in Table 3. Using the single mode approximation, the resulting modified capacitance \tilde{C}_p^{eS} can be determined by Eq. (7) by mapping the corresponding entries in the system stiffness matrix in ANSYS[®]. However, mapping the correct entries in the stiffness matrix is a heavy and rather complicated task in ANSYS[®], which uses three different layers of ordering. Therefore, it may be advantageous simply to solve the two static problems, associated to Eqs. (16) and (17) in order to get Q_s and V_s , and to determine the quasi-static capacitance C_s . In the present case, the resulting modified capacitance is found to be $\tilde{C}_p^{eS} = 616.2\text{nF}$, from which the modal EMCC κ_0^2 (Eq. (15)) follows by multiplication of its inverse with Q_r^2/ω_r^2 in Table 3.

The performance of the tuning methods based on the effective, quasi-static and modal EMCC is now analysed by considering the frequency response plot (FRP) around the first and fourth resonant frequencies, which are shown in Figure 6. It can be seen from Figure 6 that the tuning based on the effective EMCC (solid line) gives an optimum response around the resonant frequencies with a flat (unit) plateau for the shunt voltage response. The latter is observed when an idealised harmonic modal load is used for producing the FRP. This modal load is determined from the mass matrix, the SC mode shape and the modal charge as $\{F\}_r = [M]\{U\}_r Q_r$. The tuning based on the quasi-static EMCC (dashed line in Figure 6) is also seen to perform relatively well (with small deviations to the optimum shunt tuning). However, the tuning based on the modal EMCC (dashed-dotted line) is seen to be very poor in the given example causing large dynamic amplification around the original SC resonance frequency. Hence, an accurate description of the electromechanical structure, accounting for the non-resonant modes, is apparently of

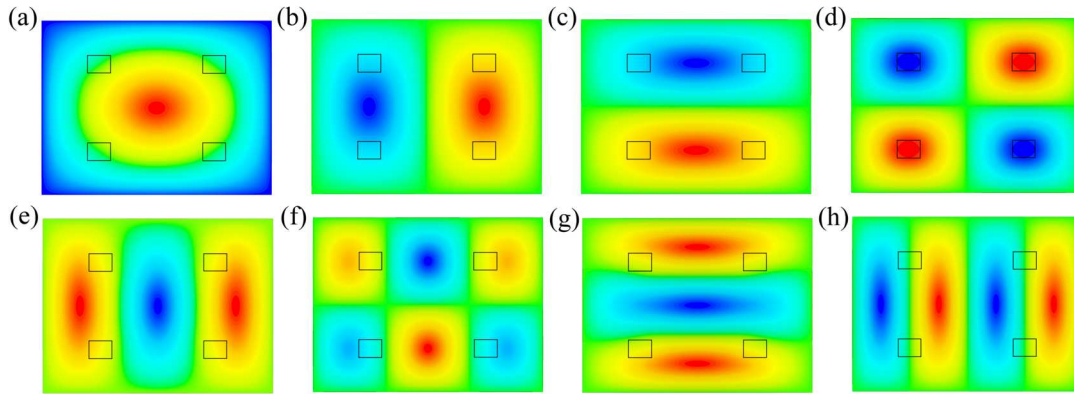


Figure 7: Mode shapes of a simply supported plate with four pairs of SC patches.

great importance as it furthermore results in a relatively simple tuning procedure.

7.2 Simply supported plate with four pairs of patches

It may be of general interest to place piezoelectric patches at decentralized location on the host structure, while maintaining the same level of supplemental modal damping. This can be realized by the application of several interacting piezoelectric patches, which further may have the potential of increasing the number of vibration modes with attainable damping, as investigated in the following for the simply supported plate. The second example thus concerns the same simply supported plate but with four pairs of piezoceramic patches placed symmetrically in the quarter points of the plate. The pairs are only a quarter of the size of the former single pair, whereby the piezoceramic volume is unchanged. The aim of the present example is to demonstrate the performance of the piezoelectric shunt damping when having several patches and to investigate the difference between having an individual patch and a network of wired patches.

As in the first example, the first eight vibration modes are exploited and shown in Figure 7 with the position of the piezoceramic SC patches indicated by the black rectangles. It can be seen from the mode shapes in Figure 7, compared to those in Figure 5, that modes 4 and 5 have interchanged. Also, the piezoceramic patches are in the present case seen to alter the vibration modes less compared to the first example, in particular for modes 7 and 8.

The SC and OC frequencies, effective EMCC, squared normalized modal charge, and parallel (p) and series (s) shunt tunings are now determined for the plate with four individually shunted pairs of patches and provided in Table 4. As the pairs of patches are symmetrically (or anti-symmetrically) positioned with respect to the deformation pattern of the first eight vibration modes, see Figure 7, the optimum tuning of each pair of patches will be identical and determined according to Appendix A. In Table 4, the provided modal charge and shunt tunings are thus for a single patch pair. It can be seen from Table 4 that damping is attainable for the first seven vibration modes given in bold-face. This is a considerable improvement compared to the three modes with substantial damping in the first example (Section 7.1). Vibration mode 8 is again seen to have vanishing attainable damping since the patches locations in Figure 7(h) are at nodal points. The effective EMCC is seen to be lower for modes 1, 5 (4 in first example) and 7 compared to the first example, which is therefore superior for these specific modes. Furthermore, it is seen that the magnitude of the optimum electronic components are considerably larger compared to the tuning in the first example. This is mainly due to the much lower modal

Table 4: SC and OC frequencies, effective EMCC, normalized modal charge and optimum RL -shunt tunings for each individual shunted pair of piezoceramic patches, for the simply supported plate with four pairs of same poled and parallel wired piezoceramic patches.

Mode (type)	f [Hz]	\hat{f} [Hz]	κ_e^2 [%]	$Q_r^2/\omega_r^2 \left[n \left(\frac{C_s}{rad} \right)^2 \right]$	L_p [H]	R_p [k Ω]	L_s [H]	R_s [k Ω]
1 (1,1)	38.58	38.66	0.41	0.141	123.1	330.8	122.1	2.678
2 (2,1)	78.24	78.64	1.01	0.348	30.09	104.0	29.49	2.073
3 (1,2)	109.3	109.8	0.93	0.321	15.36	77.36	15.08	1.420
4 (2,2)	143.3	144.7	1.90	0.648	9.049	41.77	8.714	1.545
5 (3,1)	153.0	153.5	0.62	0.216	7.821	67.28	7.725	0.833
6 (3,2)	219.8	220.9	0.98	0.334	3.840	37.92	3.766	0.731
7 (1,3)	236.3	236.9	0.52	0.178	3.295	48.06	3.261	0.494
8 (4,1)	254.6	254.6	0.00	0.000	3.253	-	3.253	-

charges caused by the smaller individual patch volumes with less conversion into electrical energy. However, this can be changed by connecting the four pairs of patches to a single common shunt. This causes the squared modal charges to increase by a factor sixteen, while the optimum tuning values for the electronic components will be a quarter of the values provides in Table 4. The attainable damping will remain unchanged, since the SC and OC frequencies and thus the effective EMCC are the same. However, attention has to be paid to the connection of the four pairs of patches as the particular configuration depends on the shape of the vibration mode to be damped. For example, for the first vibration mode, the interface (top and bottom) electrodes and the inner electrodes should be connected, respectively, and wired in parallel to the shunt circuit. This is because the in-plane strains of all the patches have equal sign. However, this is not the case for modes 2, 3, 4 and 6, for which the in-plane strains have opposite signs. These signs, and thereby the wiring of the four pairs of patches, can be determined by considering the signs of the individual modal charges. For instance, in mode 2, the modal charges of the two pairs of patches to the left are positive while they are negative for the pairs to the right, see Figure 7(b). This implies that the interface electrodes of the left patch pairs should be connected to the inner electrodes of the corresponding right patch pairs and vice versa. When the wiring of the patches is done correctly, it is apparently beneficial to connect the four pairs of patches in a single network, requiring smaller optimum shunt components.

8 Summary and conclusions

In the present work, a newly proposed RL shunt calibration procedure based on the effective EMCC is generalized and demonstrated suitable for implementation in the commercial ANSYS® FE code. The calibration procedure includes the effects of the non-resonant vibration modes, which are assumed to contribute by flexibility and inertia effects. These non-resonant effects can be determined by solving three eigenvalue problems associated with SC and OC piezoceramic patch electrodes and when a shunt circuit consisting of an inductance is introduced. However, the latter eigenvalue problem is found unnecessary to evaluate in all desired cases where the effective EMCC, and thereby the attainable damping, is significant. An alternative method based on a quasi-static EMCC is also proposed which may be of interest for a tuning based on experiments and also when computational costs are a limiting factor in the numerical analysis. The optimum tuning formulae for parallel and series shunt circuits are based on a balanced calibration principle, where the roots in the pure inductive limit appear as inverse points with respect to the SC and OC frequencies, respectively.

In the numerical examples, a smart plate benchmark is analysed for two patch pairs configura-

tions, consisting of either a single centralized pair of piezoelectric patches or four decentralised, but symmetrically placed, patch pairs. A convergence study has been carried out, for the former configuration, to demonstrate that a precise numerical model is important in order to accurately determine the effective EMCC. The first eight vibration modes have then been analysed with both patch designs and the optimum shunt circuit calibrations were determined for each individual mode. For the single patch pair design, non-vanishing damping was observed for three of the first eight vibration modes, while this increased to seven modes for the second design with four symmetric pairs. It has been demonstrated that the optimum shunt tuning causes a nearly flat plateau in the frequency response around the target resonant mode, when applying a representative modal harmonic load. Furthermore, the voltage response is found to have a completely flat (unit) plateau as dictated by the principle of equal modal damping. Finally, it was found that larger tuning values are required for the plate with four patch pairs shunted individually. However, by connecting the four pairs of patches in a single network, these tuning values can be reduced by a factor four since the modal charge increases by a factor sixteen. It is noted that close attention has to be given to the particular wiring of the patch pairs electrodes, according to the signs of the individual modal charges.

Acknowledgement

This research has been supported by the Danish Council for Independent Research via the project ‘Resonant Piezoelectric Shunt Damping of Structures’. The authors gratefully acknowledge this support.

References

- [1] Høgsberg J., Krenk S. Calibration of piezoelectric RL shunts with explicit residual mode correction. *J. Sound Vib.*, **386**(2017) 65-81
- [2] Forward R.L. Electronic damping of vibrations in optical structures. *Appl. Optics* **18**(1979) 690-697.
- [3] Hagood N.W., von Flotow A. Damping of structural vibrations with piezoelectric materials and passive electrical networks. *J. Sound Vib.* **146**(1991) 243-268.
- [4] Wu S.Y. Piezoelectric shunts with a parallel R-L circuit for structural damping and vibration control. *In Proc. SPIE* **2720**(1996) 259-269.
- [5] Krenk S., Høgsberg J., Tuned resonant mass or inerter-based absorbers: Unified calibration with quasi-dynamic flexibility and inertia correction. *Proc. Roy. Soc. A*, **472**(2016) paper no. 20150718 (23pp).
- [6] Toftekær J.F., Benjeddou A., Høgsberg J., Krenk S., Optimal piezoelectric RL shunt damping of plates with residual mode correction. *J. Intell. Mater. Syst. Struct.* **29**(2018) 3346-3370.
- [7] Trindade M., Benjeddou A. Effective electromechanical coupling coefficients of piezoelectric adaptive structures: critical evaluation and optimization. *Mech. Adv. Mater. Struct.* **16**(2009) 210-223.
- [8] Belloli A., Ermanni P. Optimum placement of piezoelectric ceramic modules for vibration suppression of highly constrained structures. *Smart Mater. Struct.* **16**(2007) 1662-1671.
- [9] Berardengo M., Thomas O., Giraud-Audine C., Manzoni S. Improved resistive shunt by means of negative capacitance: new circuit, performances and multi-mode control. *Smart Mater. Struct.*, **25**(2016) paper no. 075033 (23pp.).
- [10] Lossouarn B., Aucejo M., Deü J.-F., Multon B. Design of inductors with high inductance values for resonant piezoelectric damping. *Sens. Act. A: Phys.* **259**(2017) 68-76.
- [11] Lossouarn B., Deü J.-F., Kerschen G., A fully passive nonlinear piezoelectric vibration absorber. *Phil. Trans. Roy. Soc. A* **376**(2018) paper no. 2017014268 (16pp).
- [12] ANSYS 18.0 Documentation. ANSYS, Inc, Canonsburg, Pennsylvania, USA (2017)

- [13] Toftekær J.F., Benjeddou A. Høgsberg J. New piezoelectric shunt tuning method based on the effective electromechanical coupling coefficient: validation and 3D implementation. In A. Benjeddou and Z. Aboura (Editors), *Proc. 7th Int. Symp. Aircraft Mater.*, pp. 351-362, 2018..
- [14] Benjeddou A. Modal effective electromechanical coupling approximate evaluations and simplified analyses: Numerical and experimental assessments. *Acta Mech.* **225**(2014) 2721-2742.
- [15] Choi S. B., Kim H. S., Park J. S., Multi-mode vibration reduction of a CD-ROM drive base using a piezo-electric shunt circuit. *J. Sound Vib.* **300**(2007) 160-175.
- [16] Seba B., Ni J., Ni Lohmann, B. Vibration attenuation using a piezoelectric shunt circuit based on finite element method analysis. *Smart Mater. Struct.* **15**(2006) 509-517.
- [17] Bachmann F., Bergamini A. E., Ermanni P., Optimum piezoelectric patch positioning: A strain energy-based finite element approach. *J. Intell. Mater. Syst. Struct.* **23**(2012) 1575-1591.
- [18] Golub G. H., van Loan C. F., Matrix Computations, 2nd Edition. *The Johns Hopkins University Press*, Baltimore, USA, 1989.
- [19] Krenk S. Frequency analysis of the tuned mass damper. *J. Appl. Mech.* **72**(2005) 936-942.
- [20] Høgsberg J and Krenk S. Balanced calibration of resonant shunt circuits for piezoelectric vibration control. *J. Intell. Mater. Syst. Struct.* **23**(2012) 1937-1948.
- [21] eFunda Portal *Lead Zirconate Titanate (PZT-5H)* (2017), (available: http://www.efunda.com/materials/piezo/material_data/matdata_output.cfm?Material_ID=PZT-5H).

Appendix A: Identical and symmetrically placed pairs of piezoceramic patches

The proposed shunt tuning procedure and its implementation in ANSYS® for a single pair of patches are here extended to the case of several identical and symmetrically placed pairs of piezoceramic patches, whereby the optimum shunt tuning is the same for each pair of patches. The coupling vector $\{k_{me}^E\}$ in Eq. (6) becomes a coupling matrix $[k_{me}^E]$ with columns equal to the number of individually shunted patch pairs, while the scalar quantity $\bar{C}_p^{\epsilon S}$ becomes a diagonal matrix $\bar{C}_p^{\epsilon S}[I_n]$ containing the identical capacitive properties. At last, the variables V and Q become vectors $\{V\}$ and $\{Q\}$ with entries equal to the number of shunted patch pairs. The SC eigenvalue problem is the same as for the single piezoceramic patch pair (Eq. (9)), while the sensor equation is given as

$$\{Q_j\} = -[k_{me}^E]^t \{U\}_j \quad (57)$$

It is seen that the modal charge becomes a vector containing the individual modal charges for each shunted patch pair, which are now collected in the modal charge matrix

$$[Q]^t = [\{Q_1\} \quad \{Q_2\} \quad \cdots \quad \{Q_n\}] \quad (58)$$

The modal equations Eqs. (21)-(22) are then, for n shunted pairs of patches and the r 'th mode, given as

$$(\omega_r^2 - \omega^2)v_r = \{Q_r\}^t \{V\} \quad (59)$$

$$\bar{C}_p^{\epsilon S}[I_n]\{V\} - \{Q\} = -[Q]^t \{v\} \quad (60)$$

The right hand side of Eq. (60) is approximated similarly to Eq. (23) as

$$[Q]^t \{v\} = \{Q_r\}v_r + \left(C_r' - \frac{1}{\omega^2 L_r'}\right)[I_n]\{V\} \quad (61)$$

Table 5: Parallel and series shunt tuning for identical and symmetrically placed pairs of piezoceramic patches.

Parallel	Series
$L = \frac{\kappa_e^2}{nQ_r^2}, \quad R = \frac{\kappa_e^2 \omega_r}{nQ_r^2} \sqrt{\frac{1}{2\kappa_e^2}}$	$L = \frac{\kappa_e^2}{nQ_r^2(1 + \kappa_e^2)^2}, \quad R = \frac{\kappa_e^2 \omega_r}{nQ_r^2} \sqrt{\frac{2\kappa_e^2}{(1 + \kappa_e^2)^3}}$

whereby the governing equation follows by eliminating $\{Q_r\}v_r$ between Eqs. (59) and (61)

$$\left[\left(\bar{C}_p^{\epsilon^S} + C_r' - \frac{1}{\omega^2 L_r'} \right) (\omega_r^2 - \omega^2) [I_n] + \{Q_r\} \{Q_r\}^t \right] \{V\} = \{Q\} (\omega_r^2 - \omega^2) \quad (62)$$

For identical and symmetrically placed patches, with respect to the deformation pattern of the target vibration mode, Eq. (62) represents the number of shunt circuits n redundant equations given as

$$\left[\left(\bar{C}_p^{\epsilon^S} + C_r' - \frac{1}{\omega^2 L_r'} \right) (\omega_r^2 - \omega^2) + nQ_r^2 \right] V = Q (\omega_r^2 - \omega^2) \quad (63)$$

in which Q_r^2 is the common squared modal charge, while Q and V are the common circuit charges and electric potentials, respectively.

Finally, use of Ohm's law in Eq. (43) gives the characteristic equation

$$\left[\frac{\omega^2}{\omega_r^2} - (1 + \kappa_r^2) \left(1 - \frac{\kappa_r^2}{\kappa_e^2} \right) - i\omega \frac{1}{Z_{sh}(\omega) nQ_r^2} \kappa_r^2 \right] \left(1 - \frac{\omega^2}{\omega_r^2} \right) + \kappa_r^2 \frac{\omega^2}{\omega_r^2} = 0 \quad (64)$$

which is similar to Eq. (44) but with nQ_r^2 instead of Q_r^2 . The effect on the individual shunt tunings is thus the factor n on the modal charge Q_r^2 , whereby the optimum shunt tunings are given as listed in Table 5.

Appendix B: Determination of κ_e^2 from quadratic equation (25)

Initially Eq. (25) is multiplied with $-\hat{\omega}_r^2/C_r$, whereby one obtains the quadratic equation

$$\left(-\hat{\omega}_r^2 + \frac{1}{C_r L_r'} \right) (\omega_r^2 - \hat{\omega}_r^2) - \hat{\omega}_r^2 \frac{Q_r^2}{C_r} = 0 \quad (65)$$

Division with ω_r^4 and using Eqs. (28)-(29), Eq. (65) transform above relation to

$$\left[-\left(\frac{\hat{\omega}_r}{\omega_r} \right)^2 + \kappa_r^2 \lambda_r' \right] \left[1 - \left(\frac{\hat{\omega}_r}{\omega_r} \right)^2 \right] - \left(\frac{\hat{\omega}_r}{\omega_r} \right)^2 \kappa_r^2 = 0 \quad (66)$$

Now, after using Eq. (13), the characteristic equation is obtained in terms of the effective EMCC as

$$\left(1 + \kappa_e^2 - \kappa_r^2 \lambda_r' \right) \kappa_e^2 - \kappa_r^2 \left(1 + \kappa_e^2 \right) = 0 \quad (67)$$

Which can be written in a quadratic form as

$$(\kappa_e^2)^2 + \left(1 - \kappa_r^2 - \lambda_r' \kappa_r^2 \right) \kappa_e^2 - \kappa_r^2 = 0 \quad (68)$$

This is a quadratic equation in κ_e^2 that can be solved in order to find κ_e^2 when both correction terms are included. However, it is of interest to find a solution that can be truncated for $\lambda_r' \simeq 0$.

Thus, instead, Eq. (68) is solved with respect to $\Delta\kappa^2 = \kappa_e^2 - \kappa_r^2 \rightarrow 0$ for $\lambda'_r \rightarrow 0$. Using the former relation, the following holds

$$(\kappa_e^2)^2 = \left(\Delta\kappa^2 + \kappa_r^2\right)^2 = (\Delta\kappa^2)^2 + 2\kappa_r^2\Delta\kappa^2 + (\kappa_r^2)^2 \quad (69)$$

Then, elimination of κ_e^2 between Eqs. (68) and (69) gives

$$(\Delta\kappa^2)^2 + \left(1 + \kappa_r^2 - \lambda'_r\kappa_r^2\right)\Delta\kappa^2 - (\kappa_r^2)^2\lambda'_r = 0 \quad (70)$$

For $\lambda'_r \rightarrow 0$, Eq. (70) reduces to

$$\Delta\kappa^2 = -(1 + \kappa_r^2) \quad \text{or} \quad \Delta\kappa^2 = 0 \quad (71)$$

while the full solution can be found as

$$\Delta\kappa^2 = \frac{1}{2}\left(1 + \kappa_r^2 - \lambda'_r\kappa_r^2\right) \left[\sqrt{1 + \frac{4(\kappa_r^2)^2\lambda'_r}{(1 + \kappa_r^2 - \lambda'_r\kappa_r^2)^2}} - 1 \right] \quad (72)$$

whereby the effective EMCC κ_e^2 follows by Eq. (27).

Appendix C: Derivation of characteristic equation (52) for series shunt connection

Initially, the series shunt circuit impedance $Z_{sh}(\omega)$ in Eq. (51) is inserted in the characteristic equation (44), followed by the elimination of the inductance and resistance through the normalized inductance in Eq. (36) and electric damping parameter in Eq. (53). Thus, the characteristic equation (44) can hereby be written as

$$\left[\left(\frac{\omega}{\omega_r}\right)^2 - (1 + \kappa_r^2)\left(1 - \frac{\kappa_r^2}{\kappa_e^2}\right) + \omega^2 \frac{\lambda_r\kappa_r^2}{i\omega\rho_r^s\lambda_r - \omega^2} \right] \left[1 - \left(\frac{\omega}{\omega_r}\right)^2 \right] + \kappa_r^2 \left(\frac{\omega}{\omega_r}\right)^2 = 0 \quad (73)$$

The characteristic equation (73) is now multiplied by $(i\omega\rho_r^s\lambda_r - \omega^2)/\omega^2$ whereby the former, after using Eq. (39), can be written as

$$\left\{ i\left(\frac{\omega}{\omega_r}\right)\rho_r^s\frac{\lambda_r}{\omega_r} \left[1 - \left(\frac{\omega_r}{\omega}\right)^2 (1 + \kappa_r^2) \left(1 - \frac{\kappa_r^2}{\kappa_e^2}\right) \right] + \lambda_r^*\kappa_r^2 - \left(\frac{\omega}{\omega_r}\right)^2 \right\} \left[1 - \left(\frac{\omega}{\omega_r}\right)^2 \right] + i\left(\frac{\omega}{\omega_r}\right)\rho_r^s\frac{\lambda_r}{\omega_r}\kappa_r^2 - \kappa_r^2\left(\frac{\omega}{\omega_r}\right)^2 = 0 \quad (74)$$

Finally, the products in Eq. (74) are expanded and this characteristic equation can be written as

$$\begin{aligned} & \left(\frac{\omega}{\omega_r}\right)^4 - \left(1 + \kappa_r^2 + \lambda_r^*\kappa_r^2\right)\left(\frac{\omega}{\omega_r}\right)^2 + \lambda_r^*\kappa_r^2 \\ & + i\left(\frac{\omega}{\omega_r}\right)\rho_r^s\frac{\lambda_r}{\omega_r} \left[1 + \kappa_r^2 - \left(\frac{\omega}{\omega_r}\right)^2 - (1 + \kappa_r^2)\left(1 - \frac{\kappa_r^2}{\kappa_e^2}\right)\left(\frac{\omega_r^2}{\omega^2} - 1\right) \right] = 0 \end{aligned} \quad (75)$$

In order to identify the inverse points relation, it is convenient to multiply Eq. (75) by $1/(1 + \kappa_e^2)^2$ and use the relation $1/(1 + \kappa_e^2) = (\omega_r/\hat{\omega}_r)^2$ from Eq. (13). Hereby, the characteristic equation (75) can be written as in Eq. (52).